Radiation Science and Technology
2026, Vol. 12, No. 3, pp. 52–63
https://doi.org/10.11648/j.rst.20261203.12

Research Article

Measurement and Evaluation of Organ Dose in Patients Using Anthropomorphic Phantom During Intravenous Urography Procedure in Yobe State, Nigerian Hospitals

Yakubu Mohammed Tukur*, Nuraddeen Nasir Garba, Anas Muhammad Salisu, Usman Musa Kankara, Aisha Ahmed

Department of Physics, Ahmadu Bello University, Zaria, Nigeria

Abstract

Intravenous urography (IVU) remains a frontline investigation for urinary tract disease in resource-limited settings, yet organ-level dose data from north-eastern Nigeria are scarce. This study quantified absorbed doses to the kidneys, adrenal glands, ureters and bladder wall during IVU at Yobe State University Teaching Hospital (YSUTH) and Yobe State Specialist Hospital Damaturu (YSSHD), and estimated the associated cancer risk. Fifty adult patients, twenty-five from each centre, were recruited consecutively. Organ doses were measured using calibrated LiF:Mg,Ti thermoluminescent dosimeters placed inside an adult anthropomorphic phantom, and were independently estimated with CalDose_X, a Monte Carlo code based on MASH and FASH phantoms. Cancer risk was calculated from risk-weighted organ equivalent doses. The kidneys received the highest dose at both hospitals (0.352 ±0.150 mGy at YSSHD; 0.218 ±0.033 mGy at YSUTH), whereas the bladder wall received the lowest, about 0.010 mGy. Doses were consistently higher at YSSHD, which coincided with higher tube potentials, larger current–time products and older equipment. Estimated cancer risks ranged from 1.58×10^{-6} to 3.66×10^{-6}. Although all doses were far below the 10 mGy reference level, female risks approached the ICRP benchmark (35 per million). Harmonized protocols, equipment renewal and local reference levels are warranted.

Keywords

Intravenous Urography, Anthropomorphic Phantom, Thermo-luminescent Dosimeters, CALDose_X 5.0 Model, Yobe State University Teaching Hospital, Yobe State Specialist Hospital Damaturu, Radiation-induced Cancer

1. Introduction

Medical imaging is now the dominant artificial contributor to population exposure from ionizing radiation, and in high-income countries it accounts for roughly half of the total dose received from all sources combined [1]. The share attributable to diagnostic radiology has grown steadily as imaging capacity has expanded, and although computed tomography dominates collective dose in well-resourced systems, conventional radiography and fluoroscopy still account for the majority of individual examinations performed worldwide. This distinction matters for radiation protection policy in low- and mid-

*Correspondence: Yakubu Mohammed Tukur (mtukury@gmail.com)

Received: 20 July 2026; **Accepted:** 3 August 2026; **Published:** 23 November 2026

Copyright: © The Author(s), 2026. Published by Science Publishing Group. This is an **Open Access** article, distributed under the terms of the Creative Commons Attribution 4.0 License (http://creativecommons.org/licenses/by/4.0/), which permits unrestricted use, distribution and reproduction in any medium, provided the original work is properly cited.

dle-income settings, where the equipment mix, the maintenance regime and the prevailing technique factors differ appreciably from those on which international dose surveys are built.

Uroradiology emerged almost immediately after Röntgen's discovery, initially for the detection of urinary tract calculi, and the introduction of iodinated contrast media in the 1920s and 1930s established intravenous urography (IVU) as the reference investigation of the urinary tract for most of the twentieth century [2, 3]. Computed tomography urography and ultrasonography have since displaced IVU in many centres, yet the older technique persists where cost, equipment availability and power supply constrain practice [4]. It remains diagnostically useful for obstructive uropathy, for the assessment of collecting system anatomy and for the localization of calculi, and it continues to be requested routinely across much of West Africa. Its dosimetric significance lies less in any single exposure than in the structure of the examination: a control radiograph is followed by a nephrogram and by a sequence of delayed films, so that the same abdominal volume is irradiated five or six times within about half an hour.

Conventional dose descriptors do not capture that burden in a form useful for risk estimation. Entrance surface dose and effective dose are convenient and comparable across centres, but the first reports only the skin, and the second collapses the distribution of energy deposition across the body into a single population-averaged, sex-averaged quantity [5]. Neither supports a statement about the probability of renal or bladder malignancy in the individual exposed. Organ absorbed dose, by contrast, is the quantity to which the epidemiological risk models are anchored, and it is therefore the quantity required if the justification of a procedure is to be argued on anything more than custom [5, 6].

Two routes to organ dose are available. Direct measurement places calibrated dosimeters within an anthropomorphic phantom whose tissue-equivalent composition and embedded skeleton reproduce the attenuation and scatter conditions of a real abdomen [7, 8]. Its strength is that it interrogates the actual X-ray unit, beam quality and geometry in use at a given site; its weaknesses are cost, labour and the fact that a single phantom represents a single body habitus. The computational route substitute's conversion coefficients precomputed by Monte Carlo transport in reference phantoms, and returns organ doses from recorded exposure factors without any additional irradiation [9]. CalDose_X, developed at the Department of Nuclear Energy in Recife, is among the most widely applied implementations; version 5.0 draws its coefficients from the MASH and FASH mesh-based adult phantoms in both standing and supine posture, which is a material improvement on the earlier MIRD-type mathematical models and on image-derived voxel phantoms whose organs are displaced by the supine scanning position [9-12]. Recent applications confirm its continuing utility: Paula and colleagues used it to establish age-stratified organ doses in paediatric abdominal and pelvic radiography following a digital equipment upgrade [13], while comparisons against thermoluminescent measurement in physical phantoms report agreement within roughly 50 per cent for organs lying in the primary beam and poorer concordance at the field periphery [14].

The recent literature on organ-level dosimetry in projection radiography is otherwise concentrated in North Africa, the Middle East and East Asia. Yamashita and co-workers measured organ doses directly during diagnostic computed tomography, reporting 12.04 mGy to the kidney and 15.53 mGy to the lung [15]. Akyea-Larbi and colleagues compared phantom measurement with a commercial dose calculator and obtained values from 3.97 mGy for the oesophagus to 56.22 mGy for the brain, some of which exceeded accepted reference levels [16]. Sina and co-workers, using TLD-100H chips in a RANDO phantom, mapped organ dose distributions for chest, pelvic and skull radiography and concluded that indirect estimation from calibrated tube output reproduces direct measurement closely enough to be preferred for national reference-level surveys, given the cost of phantom work [17]. Elamri and colleagues reached broadly similar conclusions for four digital radiography procedures using optically stimulated luminescence dosimeters in a Moroccan hospital [18], and Layal and co-workers reported patient doses for contrast-enhanced computed tomography urography [19]. What is missing from this body of work is any organ-level assessment of conventional IVU in Nigeria.

The Nigerian dosimetry literature is thin and, where it exists, restricted to surface quantities. Zira established diagnostic reference levels for radiological procedures in teaching hospitals in the north-east [20]; Bullus and colleagues evaluated patient doses at two public hospitals in Damaturu [21]; Odunayo estimated doses for selected examinations in the north-central states [22]; and Suliman and co-workers surveyed IVU doses in Sudan with a view to optimisation [23]. All report entrance surface or dose-area product values. A companion study by the present authors established entrance surface and effective doses for IVU at the same two Yobe State facilities [24], but stopped short of organ-level measurement. No published work, to our knowledge, reports measured organ absorbed doses for IVU anywhere in north-eastern Nigeria, and no locally derived diagnostic reference level exists for the procedure.

This study was designed to close that gap. Its objectives were, first, to measure absorbed doses to the kidneys, adrenal glands, ureters and bladder wall during IVU at two referral hospitals in Yobe State using thermoluminescent dosimetry in an anthropomorphic phantom; second, to estimate the same quantities independently with CalDose_X 5.0 and examine the agreement between the two methods; third, to derive sex-specific radiation-induced cancer risks and set them against the benchmarks of the International Commission on Radiological Protection; and fourth, to propose candidate local diagnostic reference levels. The two facilities were chosen precisely because their equipment differs in age and specification, which permits the influence of equipment condition on patient dose

to be examined without confounding by patient population. The work is intended to furnish baseline data for optimization under the ALARA principle and to inform the targeted quality-improvement measures that the results indicate are needed.

2. Materials and Methods

2.1. Study Design, Setting and Ethical Approval

A facility-based cross-sectional study was carried out at two referral hospitals in Yobe State, north-eastern Nigeria: Yobe State University Teaching Hospital (YSUTH) and Yobe State Specialist Hospital Damaturu (YSSHD). Between them these centres handle most of the IVU workload in the state, and their radiographic units differ appreciably in age and specification. Data collection ran from September, 2024 to January, 2025.

The protocol was approved by the Health Research Ethics Committees of both institutions (approval numbers; YSUTH/MAC/EA/077/VOL/765 and YSSH/GEN/DTR/013) and the study was conducted in accordance with the principles of the Declaration of Helsinki. Written informed consent was obtained from every participant after the purpose of the work had been explained in English or Hausa. No patient received any radiation beyond that required for their clinically indicated examination: exposure factors were recorded from patients, whereas the irradiations used for dose measurement were delivered to a phantom.

2.2. Patient Recruitment and Data Collection

Fifty adults, twenty-five at each hospital, were recruited by consecutive sampling. Eligibility required an age of at least 18 years, a clinical indication for IVU, and a body mass index between 18.5 and 30.0 kg m^{-2}, the last criterion applied so that the recruited group would sit reasonably close to the reference anatomy of the phantom and of the computational models. Pregnant women, minors, and examinations that were abandoned, repeated or extended with additional projections were excluded.

Age, sex, standing height (h, m) and body mass (m, kg) were recorded on a standardized data sheet, with body mass index computed as

$$\mathrm{BMI} = m / h^2 \tag{1}$$

The exposure parameters of every projection were logged: tube potential U (kV), tube current–exposure time product It (mAs), focus-to-detector distance d_{FDD} (cm), focus-to-skin distance d_{FSD} (cm), field dimensions at the detector, projection geometry, and the number and timing of films. The standard series at both centres comprised a preliminary control radiograph followed by nephrogram, 0-minute, 5-minute, 10-minute and 15-minute films and a post-micturition view, all anterior-posterior (AP).

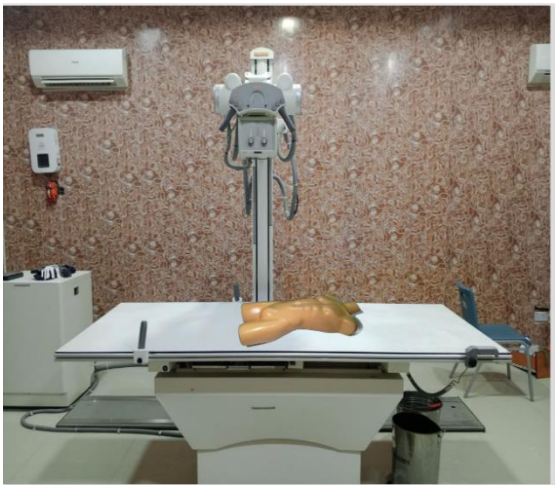


Figure 1. *Supine view of a phantom.*

2.3. Radiographic Equipment and Quality Control

Examinations at YSUTH were performed on a *Fixed type Rotanode X-ray*, model; E7239X (S/N. 11m1250), installed 2015 at radiography unit and those at YSSHD on a Mobile X-ray apparatus (100mA), model; F100(XD4-2.9/100), and was installed 2009. Before any dosimetric measurement both systems underwent quality-control assessment following IAEA and AAPM protocols [25], using a calibrated multimeter (Model; TMT5360011) traceable to a Secondary Standard Dosimetry Laboratory. Tube potential accuracy, timer accuracy, output reproducibility, output linearity and half-value layer (HVL) were verified. Units were accepted where the measured kV deviated by no more than 5 per cent from nominal, the coefficient of variation of output did not exceed 0.05, the linearity coefficient did not exceed 0.1, and the HVL was at least 2.3 mm Al at 80 kV. Measured HVL values were subsequently used to select the total-filtration setting in the Monte Carlo software, since conversion coefficients are sensitive to beam quality.

Tube output Y was measured free-in-air at a reference distance d_{ref} of 100 cm across the clinical kV range and expressed as air kerma per unit current–time product:

$$Y(d_{\mathrm{ref}}) = K_{\mathrm{air}} / (It) \tag{2}$$

2.4. Anthropomorphic Phantom and Thermoluminescent Dosimetry

Organ doses were measured in an adult anthropomorphic phantom (model; ART212A) constructed from tissue-equivalent epoxy resin around a natural human skeleton and sectioned into 25 mm transverse slices with pre-drilled cavities at manufacturer-defined organ positions [7, 8]. Dosimeter locations for the kidneys, adrenal glands, ureters and bladder wall were taken from the manufacturer's organ map rather than as-

signed by inspection, so that the measurement points are reproducible.

Lithium fluoride chips doped with magnesium and titanium (LiF:Mg,Ti, TLD-100), 3.2 × 3.2 × 0.9 mm, were used throughout. The choice reflects the near tissue-equivalence of LiF, whose effective atomic number of 8.14 is close to the 7.42 of soft tissue, which keeps the energy-dependence correction small across the diagnostic range [17]. Chips were annealed at 400 ℃ for one hour followed by 100 ℃ for two hours and read on a harshaw 500 reader under nitrogen flow from 50 to 300 ℃ at 10 ℃ s^{-1}.

Batch homogeneity was established by irradiating the full batch to a common dose and computing an element correction coefficient for each chip:

$$\mathrm{ECC}_i = M / M_i \tag{3}$$

where M_i is the reading of chip i and M the batch mean. Chips departing from the mean by more than 5 per cent were withdrawn. The reader calibration factor was obtained by exposing a sub-set of chips to a known air kerma delivered by an SSDL-traceable ionization chamber at the beam quality of interest:

$$\mathrm{RCF} = M_{\mathrm{cal}} / K_{\mathrm{cal}} \tag{4}$$

The absorbed dose registered by an individual chip follows as

$$D_{\mathrm{TLD}} = [(M_i - M_{\mathrm{bg}}) \times \mathrm{ECC}_i / \mathrm{RCF}] \times f_E \tag{5}$$

in which M_{bg} is the mean reading of unirradiated control chips transported and stored with the measurement batch, and f_E is the energy-response correction relating the mean energy of the diagnostic beam to the calibration quality. Three chips were placed at each organ location and the organ dose for a single projection taken as their arithmetic mean:

$$D_T = (1/n)\, \Sigma\, D_{\mathrm{TLD},k} \tag{6}$$

Because IVU is not a single exposure, the quantity of clinical interest is the cumulative dose across the series. For each organ this was obtained by summing over the N projections of the standard protocol:

$$D_{T,\mathrm{total}} = \Sigma_{j=1}^{N} D_{T,j} \tag{7}$$

This cumulative treatment deserves emphasis, since much of the published Nigerian dosimetry literature reports single-projection values and so understates the burden of multi-phase contrast studies [20-22].

2.5. Derivation of the Measurable Dosimetric Quantities

Incident air kerma (INAK), K_i, is the air kerma on the central beam axis at the point where that axis meets the entrance surface, excluding backscatter. It was determined from the measured tube output using the inverse-square relation:

$$K_i = Y(d_{\mathrm{ref}}) \times (It) \times (d_{\mathrm{ref}} / d_{\mathrm{FSD}})^2 \tag{8}$$

For cross-checking, and for consistency with the empirical estimator implemented in the dose-calculation software, INAK was also evaluated as

$$K_i = U^{2.5}\, (It) / 400 \tag{9}$$

with the focus-to-skin distance obtained from

$$d_{\mathrm{FSD}} = d_{\mathrm{FDD}} - t \tag{10}$$

where t is the phantom thickness along the beam axis. Entrance surface air kerma (ESAK), which includes backscattered radiation, follows as

$$K_e = K_i \times B \tag{11}$$

with B the backscatter factor, defined for a tissue-equivalent water phantom as

$$B = K_{\mathrm{es,water}} / K_i \tag{12}$$

Values of B were taken from the software's internal tables for the corresponding tube potential, total filtration and field size, and lay between 1.25 and 1.45 across the kV range encountered. The air kerma-area product was computed as

$$P_{\mathrm{KA}} = K_i \times A \tag{13}$$

with the field area at the entrance surface scaled from the collimated area at the detector plane, A_d:

$$A = A_d \times (d_{\mathrm{FSD}} / d_{\mathrm{FDD}})^2 \tag{14}$$

2.6. Monte Carlo Organ Dose Estimation Using CalDose_X 5.0

Organ absorbed doses were independently estimated with CalDose_X 5.0, which returns organ and tissue absorbed doses, effective dose and cancer risk for conventional radiographic examinations [9]. The program works from precomputed conversion coefficients (CCs) between organ absorbed dose and a measurable normalisation quantity, generated by EGSnrc transport in the MASH and FASH mesh-based adult reference phantoms in standing and supine posture [10-12]. Organ dose is therefore

$$D_T = c_{\mathrm{DT/Ki}} \times K_i \tag{15}$$

where $c_{\mathrm{DT/Ki}}$ is the conversion coefficient for the organ, projection, tube potential and total filtration concerned. Equivalent expressions normalised to ESAK or KAP are available in

the program and were used as internal consistency checks.

Three input choices require explanation, because each materially affects the result. First, the supine posture was selected, matching the position in which IVU is performed; organ absorbed doses for abdominal projections differ by as much as 60 per cent between the standing and supine configurations of these phantoms, so this is not a cosmetic setting [12]. Second, the AP projection with the standard abdominal and pelvic field position was used, and the optional 4 cm field displacement was not applied. Third, the total filtration entered was that inferred from the measured HVL of each unit rather than the manufacturer's nominal value, since the two diverge in ageing tubes. Sex-specific calculations were run separately with the MASH (male) and FASH (female) phantoms, using 5×10^6 source photons, for which the statistical uncertainty on in-beam organ doses is typically below 1 per cent [9].

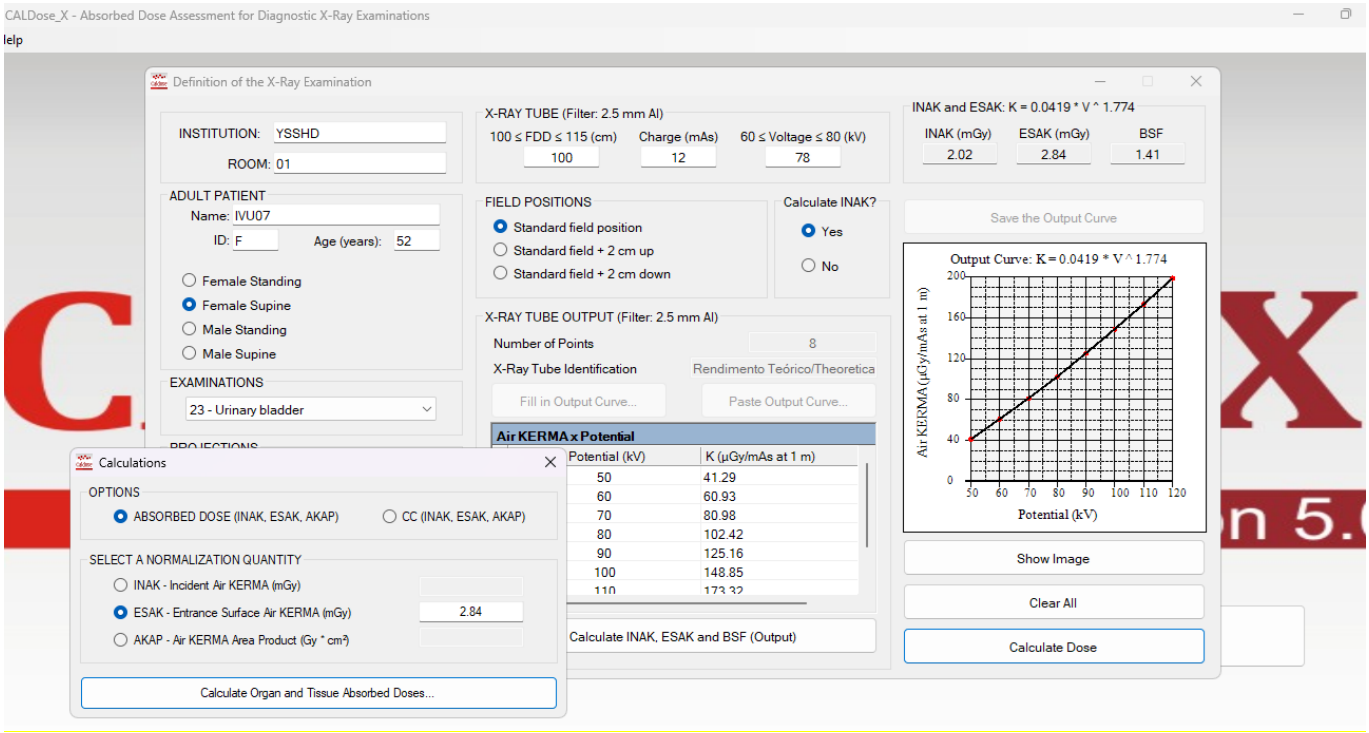


Figure 2. *Interface of CalDose_X 5.0 model.*

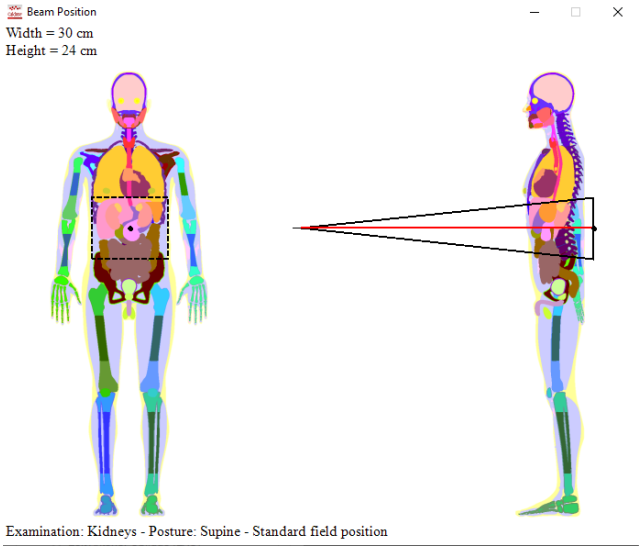


Figure 3. *Anterior-posterior and lateral view of a pelvic phantom.*

2.7. Comparison of the Measured and Computed Doses

Agreement between the two approaches was quantified for each organ as a percentage difference,

$$\Delta\,(\%) = [(D_{\mathrm{CALDose}} - D_{\mathrm{TLD}}) / D_{\mathrm{TLD}}] \times 100 \qquad (16)$$

and examined graphically by Bland–Altman analysis with limits of agreement at the mean difference ± 1.96 standard deviations. The step was included because the two methods answer slightly different questions: phantom measurement captures the actual beam, geometry and equipment behaviour at each site, whereas the Monte Carlo estimate refers to a reference anatomy. Published comparisons of this kind report agreement within roughly 50 per cent for organs in the primary beam and larger discrepancies at the field periphery [14, 16, 18].

2.8. Equivalent Dose, Effective Dose and Cancer Risk Estimation

Organ equivalent dose was obtained from absorbed dose as

$$H_T = \Sigma_R \, w_R \, D_{T,R} \tag{17}$$

with the radiation weighting factor w_R equal to unity for the photon energies involved, so that equivalent dose in Sv is numerically equal to absorbed dose in Gy. Effective dose followed as the tissue-weighted sum

$$E = \Sigma_T \, w_T \, H_T \tag{18}$$

using the tissue weighting factors of ICRP Publication 103 [26]. The radiation detriment, expressed as the probability of radiation-induced cancer attributable to the examination, was computed as the risk-weighted sum of organ equivalent doses:

$$R = \Sigma_T \, r_T \, H_T \tag{19}$$

where r_T is the lifetime tissue-specific cancer risk per unit organ equivalent dose. A nominal coefficient of 5×10^{-2} Sv^{-1} was adopted. That value remains defensible: the detriment calculation methodology was re-examined by ICRP Task Group 102 and published as ICRP Publication 152, which confirmed that the approximate overall fatal risk coefficient of 5 per cent per Sv underpinning international safety standards continues to be appropriate for protection purposes, notwithstanding the total detriment of 5.7×10^{-2} Sv^{-1} quoted in Publication 103 for the whole population and 4.2×10^{-2} Sv^{-1} for adult workers [26-29]. Sex-disaggregated risks of cancer incidence and mortality were additionally read from the software output, which applies the probability coefficients of the United States Environmental Protection Agency [30]. Results are reported separately for males and females because the risk models diverge substantially by sex for abdominal and pelvic exposures [5].

INSTITUTION: YSUTH
ROOM: 1
X-RAY TUBE (Filter: 2.5 mm Al): Rendimento Teórico/Theoretical Output
ADULT PATIENT: Male Supine Age: 39 years
Name: IVU01_EXP1h-D
ID: M
Calculation date: 24/01/2025 CALDose_X_5.0

EXPOSURE CONDITIONS
MASH3SUP: KIDNEYS, ANTERIOR-POSTERIOR (AP)
IMAGE BEHIND THE BODY
60 kVcp 2.5 mm Al 17 Deg Tungsten IPEM/SR78
MEAN SPECTRAL ENERGY: 35.6 keV ABSORBED FRACTION: 0.64
SOURCE-TO-DETECTOR (FILM): 113 cm
SOURCE-TO-SKIN: 86.0 cm
FIELD SIZE IN DETECTOR PLANE: 30 cm x 24 cm
FIELD POSITION: STANDARD POSTURE: SUPINE
MALE ADULT (ICRP89)
BODY MASS: 73.0 KG, STANDING HEIGHT: 176.0 CM
CHARGE: 8 mAs

ORGAN/TISSUE ABSORBED DOSES

ORGAN/TISSUE	mGy	%
ESAK	0.840	0.00
ADRENALS	0.031	3.12
BLADDER WALL	0.001	9.05
COLON WALL	0.125	0.83
BREASTS,glandular	0.006	8.50
KIDNEYS	0.034	1.00
LIVER	0.192	0.78
LUNGS	0.007	1.08
OESOPHAGUS	0.008	3.81
PANCREAS	0.165	0.88
SMALL INTESTINE WALL	0.053	0.85
SKIN ENTRANCE 7.2cm X 7.2cm	0.843	1.09
SPLEEN	0.101	0.94
STOMACH WALL	0.234	0.84
THYMUS	0.003	7.81
HEART WALL	0.008	1.46
LYMPHATIC NODES	0.036	0.94
GALL BLADDER WALL	0.371	1.26
SKELETON AVERAGE	0.013	0.81
MAXIMUM RBM ABSORBED DOSE	0.013	1.23
MAXIMUM BSC ABSORBED DOSE	0.017	2.44
WEIGHTED MASH DOSE	0.061	1.64
RISK OF CANCER INCIDENCE	0.28	CASES PER 100000
RISK OF CANCER MORTALITY	0.16	CASES PER 100000

Figure 4. *Dose calculation window of CalDose_X 5.0.*

2.9. Uncertainty Analysis

An uncertainty budget was constructed following the GUM framework [31]. Assuming uncorrelated input quantities, the relative combined standard uncertainty of an organ dose is

$$u_c(D_T) / D_T = \sqrt{[\, \Sigma \, (u(x_i) / x_i)^2 \,]} \tag{20}$$

And the expanded uncertainty was reported as $U = k \cdot u_c$ with coverage factor $k = 2$, corresponding to approximately 95 per cent confidence. Contributions considered were TLD reproducibility, the reader calibration factor, the energy-response correction, dosimeter positioning within the phantom, tube output measurement and, for the computational route, the Monte Carlo statistical error and the mismatch between patient and reference-phantom anatomy.

2.10. Statistical Analysis

Data were analyzed in MS excel version 13. Normality was assessed with the Shapiro–Wilk test. Normally distributed

variables are presented as mean ± standard deviation and the remainder as median with interquartile range. Differences in organ dose between hospitals were tested with the independent-samples *t*-test where normality held and the Mann–Whitney *U* test where it did not. Associations between patient size and organ dose were examined by Pearson or Spearman correlation as appropriate. A two-tailed *p*-value below 0.05 was taken as significant. In keeping with established practice, the third quartile of the distribution of ESAK and KAP at each facility was computed and proposed as a candidate local reference value [32].

3. Result and Discussions

3.1. Patient Characteristics

The two cohorts were broadly comparable, as Table 1 shows. Patients at YSSHD were on average about six years older and five centimeters taller, but body mass and body mass index differed little between the centres. Since attenuation scales principally with body thickness, and since the mean body mass index at both sites fell in the normal range, patient habitus can reasonably be excluded as the explanation for the dose differences reported below. This is an important negative finding: it isolates equipment and technique as the operative variables.

Table 1. *Demographic characteristics of the study population (mean ± SD).*

Parameter	YSUTH (n = 25)	YSSHD (n = 25)
Age (years)	43.60 ± 15.60	49.20 ± 16.80
Height (cm)	161.30 ± 6.10	166.40 ± 8.40
Body mass (kg)	60.70 ± 9.30	62.10 ± 10.20
BMI (kg m^{-2})	23.30 ± 3.90	22.50 ± 2.60

3.2. Organ Absorbed Doses

Measured organ doses across both facilities spanned 0.008 ± 0.003 mGy to 0.352 ± 0.150 mGy (Table 2). The ordering was consistent at both sites: kidneys received the highest dose, followed by the adrenal glands, then the ureters, with the bladder wall an order of magnitude below the rest. That ordering follows directly from the geometry of the AP abdominal field. The kidneys and adrenals lie centrally within the primary beam for every film in the series, whereas the bladder sits at the inferior margin of the collimated field and receives a dose dominated by scatter rather than primary radiation.

Table 2. *Mean organ absorbed doses measured at both facilities.*

Facility	Organ	Mean dose (mGy)	SD (mGy)
YSUTH	Adrenal glands	0.198	0.037
	Bladder wall	0.008	0.003
	Kidneys	0.218	0.033
	Ureters	0.061	0.013
YSSHD	Adrenal glands	0.320	0.136
	Bladder wall	0.010	0.004
	Kidneys	0.352	0.150
	Ureters	0.219	0.134

Every organ dose was higher at YSSHD. For the kidneys the increase was 61 per cent, for the adrenals 62 per cent, and for the ureters 259 per cent. The ureteric result is the most striking and the most instructive. Because the ureters run the length of the field, their dose is particularly sensitive to collimation and to the field position actually used, and a near-fourfold difference between two centres performing nominally the same examination points to divergence in practice rather than in equipment alone.

Two further features of Table 2 merit attention. First, the standard deviations at YSSHD are three to ten times those at YSUTH for the adrenals, kidneys and ureters. Wide dispersion of this kind is the signature of inconsistent technique selection, and it is arguably a more actionable finding than the difference in means: a facility with a high but tightly controlled dose can be optimized by adjusting a protocol, whereas one with a high and variable dose requires training and audit. Second, the bladder doses are very nearly equal at the two sites despite the large differences elsewhere, which is consistent with a scatter-dominated contribution that is relatively insensitive to the primary technique factors.

The difference between centres tracks the recorded exposure parameters and the age of the equipment. Higher tube potential and larger current–time products at YSSHD raise incident air kerma directly, as Equations 8 and 9 make explicit, and an ageing tube with degraded filtration produces a softer beam whose lower-energy components are absorbed in the patient without contributing usefully to the image. The measured half-value layers recorded during quality control support this interpretation. Comparable equipment-driven variation has been documented elsewhere in the region [20-22] and in recent North African work [18].

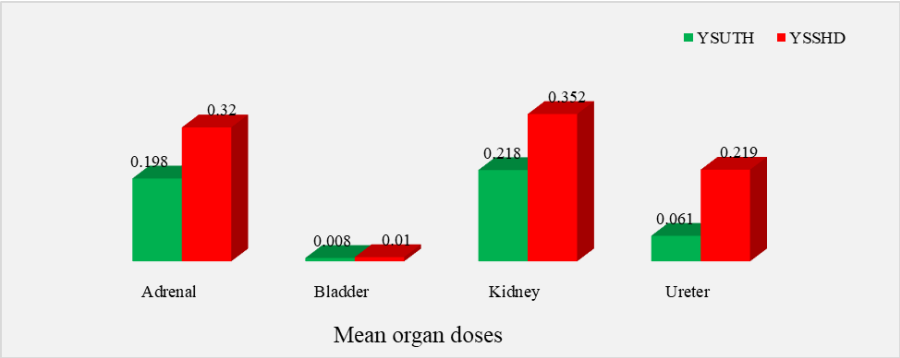


Figure 5. Mean organ doses measured in both hospitals.

3.3. Agreement Between Measurement and Monte Carlo Estimation

Doses estimated with CalDose_X 5.0 agreed with the thermoluminescent measurements to within the range reported in the validation literature for organs situated in the primary beam, and diverged more widely for the bladder wall. This pattern is expected rather than anomalous. Conversion coefficients are computed for a reference anatomy in which organ position is fixed, whereas the bladder is both mobile and peripherally sited, so a small displacement relative to the field edge produces a large fractional change in dose. Abdo and colleagues observed the same behaviour when comparing CalDose_X against thermoluminescent dosimetry in a physical phantom for chest radiography [14], and Akyea-Larbi and coworkers reported analogous discrepancies between phantom measurement and a commercial calculator [16]. The practical implication is that computational estimates are adequate for organs centrally placed in the beam, which is where most of the dose and most of the risk reside, but that phantom measurement retains its value at field margins.

3.4. Cancer Risk Estimation

Estimated probabilities of radiation-induced cancer are given in Table 3. Risks were higher for women at both facilities, by a factor of 2.3 at YSUTH and 1.6 at YSSHD.

Table 3. Estimated radiation-induced cancer risk (cases per 1000000 patients).

Facility	Sex	Cancer risk (per 10^6 patients)
YSUTH	Male	1.58 ± 0.50
	Female	3.66 ± 2.08
YSSHD	Male	2.23 ± 1.24
	Female	3.53 ± 1.72

The sex difference has a straightforward dosimetric basis and should not be read as a measurement artefact. The FASH phantom places radiosensitive pelvic organs, notably the ovaries and uterus, within or immediately adjacent to the abdominal field, and those tissues carry substantial weight in the risk models. Harrison and colleagues, analyzing effective doses and risks across diagnostic examinations by age and sex, report the same asymmetry for abdominal and pelvic procedures [5]. The finding has an operational consequence: collimation discipline and gonadal shielding matter more in women of reproductive age undergoing IVU than the sex-averaged effective dose would suggest.

Interestingly, the risk ranking between facilities does not follow the organ dose ranking. YSSHD delivered higher organ doses yet returned a slightly lower female risk than YSUTH. This apparent inconsistency arises because risk is a tissue-weighted sum over the whole body rather than a function of the four organs measured here, and because the field position and collimation recorded at the two sites differ, which alters the dose to weighted organs lying outside the measurement set. It is a useful reminder that organ dose and detriment are distinct quantities and that optimization targeting one does not automatically improve the other.

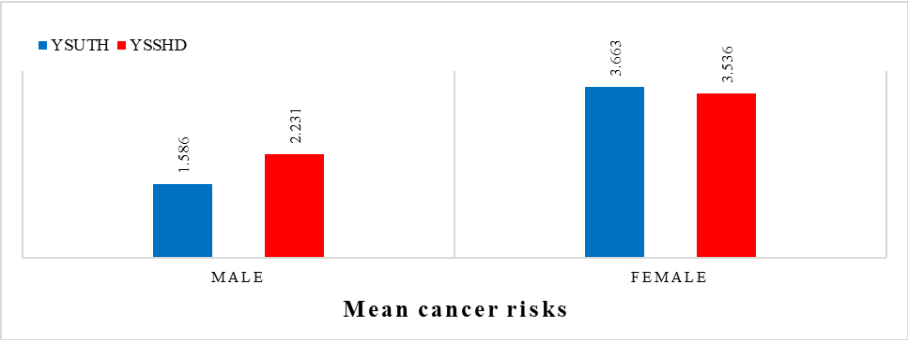


Figure 6. *Mean cancer risks in YSUTH and YSSHD.*

3.5. Comparison with Reference Levels and Published Work

All measured organ doses were far below the 10 mGy reference level applied to IVU [5, 26], by a factor of roughly thirty even for the most exposed organ at the higher-dose facility. On the dose criterion alone, the examinations performed at both centres are comfortably compliant.

The risk comparison requires more care than it is usually given. The ICRP nominal benchmark commonly invoked in this context corresponds to 35 cases per million, that is 3.5×10^{-6}. The male estimates obtained here, 1.58×10^{-6} at YSUTH and 2.23×10^{-6} at YSSHD, fall below that figure. The female estimates, 3.66×10^{-6} and 3.53×10^{-6}, do not: both sit marginally above it, and in neither case can the result be described as comfortably beneath the benchmark. Given the standard deviations in Table 3 the difference is not statistically meaningful, and the honest statement is that female risk from IVU at these facilities is at the benchmark rather than below it. Reporting it otherwise would obscure precisely the finding that most warrants attention.

Table 4. *Comparison of estimated cancer risk with published studies and reference values.*

Study	Male risk	Female risk
This study — YSUTH	$1.58 \pm 0.50 \times 10^{-6}$	$3.66 \pm 2.08 \times 10^{-6}$
This study — YSSHD	$2.23 \pm 1.24 \times 10^{-6}$	$3.53 \pm 1.72 \times 10^{-6}$
Suliman et al., Hospital A [23]	$2.70 \pm 1.01 \times 10^{-6}$	$3.46 \pm 1.20 \times 10^{-6}$
Suliman et al., Hospital B [23]	$1.06 \pm 0.83 \times 10^{-6}$	$1.71 \pm 0.97 \times 10^{-6}$
Odunayo, General Hospital Ilorin [22]	$4.20 \pm 1.43 \times 10^{-6}$	$3.78 \pm 1.11 \times 10^{-6}$
Odunayo, General Hospital Minna [22]	$2.01 \pm 0.88 \times 10^{-6}$	$2.48 \pm 0.71 \times 10^{-6}$
ICRP nominal benchmark [26]	3.5×10^{-5}	3.5×10^{-5}

Set against the comparator studies, the risks reported here are approximately an order of magnitude higher than those of Suliman and co-workers in Sudan and of Odunayo in north-central Nigeria [22, 23]. Three explanations are plausible and are not mutually exclusive. The comparator studies report doses for single projections or shorter protocols, whereas the present values are cumulative across a five- to six-film series, which alone could account for a factor of five. The technique factors in use at the Yobe State centres are higher than those reported in the comparator surveys. And the equipment at both Yobe facilities is older, with the softer beams and poorer output efficiency that follow. Disentangling these would require a prospective comparison with matched protocols, which the present cross-sectional design cannot provide.

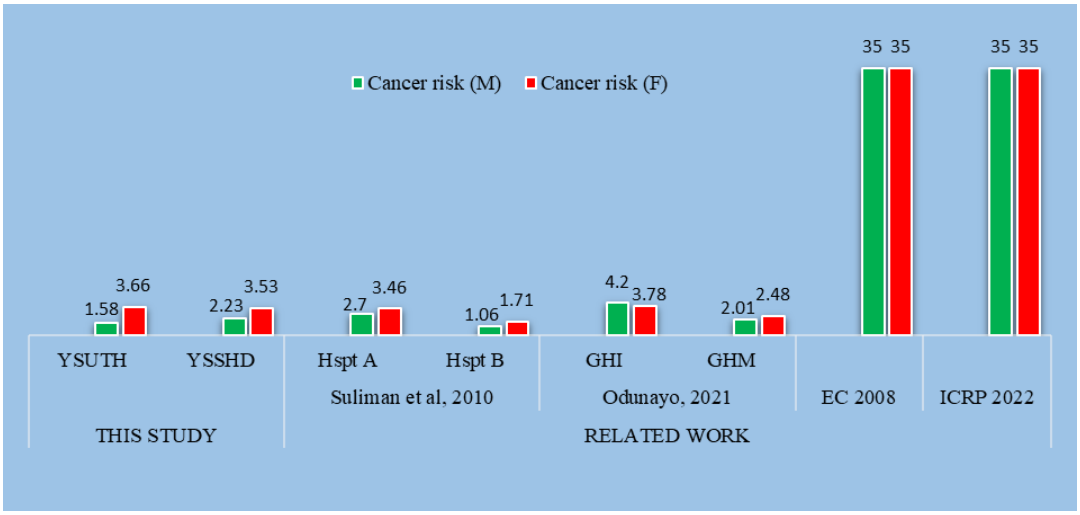


Figure 7. *Comparisons of cancer incident with related studies.*

3.6. Implications for Practice

Three actions follow from these data. Protocols should be harmonized between the two centres, with attention to the collimation practice that the ureteric doses implicate. Technique factors at YSSHD should be reviewed, since the combination of high mean dose and high dispersion indicates scope for reduction without loss of diagnostic quality, a conclusion consistent with optimization studies elsewhere [17, 18, 23]. And the equipment at YSSHD, whose age is reflected in both the doses and their variability, should be scheduled for renewal or placed under intensified quality-control surveillance. Because no locally derived diagnostic reference level exists for IVU in Nigeria, the third-quartile ESAK and KAP values obtained here are offered as candidate local reference values pending multi-centre confirmation [32].

3.7. Limitations

Several constraints qualify these findings. A single anthropomorphic phantom of fixed habitus was used, so the measured doses represent one body size and cannot be extrapolated to obese or paediatric patients, in whom attenuation and organ position differ substantially [13]. The sample of fifty patients, while adequate for characterizing technique factors at two sites, is small for establishing reference levels, which conventionally draw on larger surveys. Cancer risks are modelled quantities derived from linear no-threshold extrapolation and nominal coefficients, not observed outcomes, and they carry uncertainties considerably larger than the standard deviations quoted in Table 3, which reflect only the dispersion of the dose measurements. Finally, the study was confined to two facilities in one state and its findings should not be generalized to Nigerian practice as a whole without wider sampling.

4. Summary

This study measured organ absorbed doses during intravenous urography at two referral hospitals in Yobe State, Nigeria, a setting for which no organ-level dosimetry had been published. Fifty patients were recruited and their exposure parameters recorded, while doses to the kidneys, adrenal glands, ureters and bladder wall were measured with calibrated LiF:Mg,Ti dosimeters in an adult anthropomorphic phantom and independently estimated with CalDose_X 5.0. Doses were summed across the full five- to six-film protocol rather than reported per projection. The kidneys absorbed most, 0.352 ± 0.150 mGy at YSSHD and 0.218 ± 0.033 mGy at YSUTH, and the bladder wall least, near 0.010 mGy. Every organ dose was higher at YSSHD, with several times greater dispersion, pointing to inconsistent technique selection alongside older equipment. Estimated cancer risks were 1.58×10^{-6} and 3.66×10^{-6} for males and females at YSUTH, and 2.23×10^{-6} and 3.53×10^{-6} at YSSHD. Doses sit far below the 10 mGy reference level, but female risk estimates sit at, not below, the ICRP nominal benchmark, and all values exceed comparable African surveys by roughly an order of magnitude. The findings supply baseline data for optimization and candidate local diagnostic reference levels.

5. Conclusion

This study quantified organ-specific radiation doses during intravenous urography at Yobe State University Teaching Hospital and Yobe State Specialist Hospital Damaturu, combining thermoluminescent measurement in an anthropomorphic phantom with Monte Carlo estimation in CalDose_X 5.0. The kidneys absorbed the highest dose at both facilities, 0.352 ± 0.150 mGy at YSSHD against 0.218 ± 0.033 mGy at YSUTH, while the bladder wall received least, near 0.010

mGy. Doses were higher at YSSHD for every organ, tracking higher tube potentials, larger current–time products and older equipment rather than any difference in patient population.

Estimated lifetime cancer risks were 1.58×10^{-6} (male) and 3.66×10^{-6} (female) at YSUTH, and 2.23×10^{-6} and 3.53×10^{-6} at YSSHD. All doses fell far below the 10 mGy reference level for IVU, so the examinations are justified on dose grounds. The risk picture is less reassuring: male estimates lie below the ICRP benchmark of 35 cases per million, but female estimates sit at it rather than beneath, and all values exceed comparable Sudanese and Nigerian surveys by an order of magnitude.

Three measures follow. Protocols should be harmonized between the centres, with attention to collimation, which the ureteric doses implicate directly. Technique factors at YSSHD should be reviewed and the equipment renewed or placed under closer quality-control surveillance, since high mean dose with high dispersion indicates avoidable exposure. And because Nigeria has no local diagnostic reference level for IVU, the third-quartile values reported here offer a starting point, which multi-centre work with longitudinal follow-up should consolidate.

Abbreviations

IVU	Intravenous Urography
YSUTH	Yobe State University Teaching
YSSHD	Yobe State Specialist Hospital Damaturu
TLDs	Thermo-Luminescent Dosimeters
ICRP	International Commission on Radiation Protection
ESD	Entrance Surface Dose
ED	Effective Dose
CT	Computed Tomography
ALARA	As Low As Reasonably Achievable
BMI	Body Mass Index
FSD	Focus to Skin Distance
FDD	Focus to Detector Distance
INAK	Incident Air Kerma
ESAK	Entrance Surface Air Kerma
KAP	Air Kerma-area Product
BSF	Backscattered Factor
DRLs	Diagnostic Reference Levels
Hspt A	Hospital A
Hspt B	Hospital B
GHM	General Hospital Minna
GHI	General Hospital Ilorin

Author Contributions

Yakubu Mohammed Tukur: Conceptualization, Data curation, Formal Analysis, Investigation, Methodology, Project administration, Visualization, Writing – original draft

Nuraddeen Nasir Garba: Conceptualization, Methodology, Resources, Supervision, Validation, Writing – review & editing

Anas Muhammad Salisu: Formal Analysis, Methodology, Software, Validation, Writing – review & editing

Usman Musa Kankara: Investigation, Resources, Writing – review & editing

Aisha Ahmed: Data curation, Formal Analysis, Investigation, Writing – review & editing

Data Availability Statement

The datasets generated and analyzed during this study are available from the corresponding author on reasonable request.

Conflicts of Interest

The authors declare no conflicts of interest.

References

[1] United Nations Scientific Committee on the Effects of Atomic Radiation. Sources, effects and risks of ionizing radiation: UNSCEAR 2020/2021 report to the General Assembly, with scientific annexes. New York: United Nations; 2021.

[2] Yadav D, Dewangan R, Sharda R, Mandavi S, Pal S. Intravenous urographic study of urinary system in canine using non-ionic and ionic contrast agent. J Dairy Vet Anim Res. 2023; 12(1): 1–4. https://doi.org/10.15406/jdvar.2023.12.00315

[3] American College of Radiology, Radiological Society of North America. Intravenous pyelogram (IVP). RadiologyInfo.org; 2007.

[4] Omer H, Jambi LK, Almuwanis M, Alhasan N, Duong TT, Sulieman A, et al. Assessment of the effective radiation dose and radiogenic effect in intravenous urography imaging procedures. Radiat Phys Chem. 2022; 200: 110351. https://doi.org/10.1016/j.radphyschem.2022.110351

[5] Harrison JD, Haylock RGE, Jansen JTM, Zhang W, Wakeford R. Effective doses and risks from medical diagnostic x-ray examinations for male and female patients from childhood to old age. J Radiol Prot. 2023; 43(1): 011518. https://doi.org/10.1088/1361-6498/acbda7

[6] Lee C, Yeom YS, Shin J, Streitmatter S, Kitahara CM. NCIRF: an organ dose calculator for patients undergoing radiography and fluoroscopy. Biomed Phys Eng Express. 2023; 9(4): 045024. https://doi.org/10.1088/2057-1976/acd2de

[7] Compagnone G, Pagan L, Bergamini C. Comparison of six phantoms for entrance skin dose evaluation in 11 standard X-ray examinations. J Appl Clin Med Phys. 2005; 6(1): 101–113.

[8] Ng KH, Yeong CH. Imaging phantoms: conventional X-ray imaging applications. In: Biological and Medical Physics, Biomedical Engineering. New York: Springer; 2014.

[9] Kramer R, Khoury HJ, Vieira JW. CalDose_X — a software tool for the assessment of organ and tissue absorbed doses, effective dose and cancer risks in diagnostic radiology. Phys Med Biol. 2008; 53(22): 6437–59. https://doi.org/10.1088/0031-9155/53/22/011

[10] Cassola VF, de Melo Lima VJ, Kramer R, Khoury HJ. FASH and MASH: female and male adult human phantoms based on polygon mesh surfaces: I. Development of the anatomy. Phys Med Biol. 2010; 55(1): 133–62. https://doi.org/10.1088/0031-9155/55/1/009

[11] Kramer R, Cassola VF, Khoury HJ, Vieira JW, de Melo Lima VJ, Robson Brown K. FASH and MASH: female and male adult human phantoms based on polygon mesh surfaces: II. Dosimetric calculations. Phys Med Biol. 2010; 55(1): 163–89.

[12] Cassola VF, Kramer R, Brayner C, Khoury HJ. Posture-specific phantoms representing female and male adults in Monte Carlo-based simulations for radiological protection. Phys Med Biol. 2010; 55(15): 4399–430. https://doi.org/10.1088/0031-9155/55/15/014

[13] Paula V, Akemi Y, Hugo S, Priscila C, Rosiane M, Sergei P, et al. Organ dose estimation in pediatric abdomen and pelvic radiographs using CalDose_X Monte Carlo simulations. Radiat Phys Chem. 2025; 237: 113094. https://doi.org/10.1016/j.radphyschem.2025.113094

[14] Abdo RC, Umisedo NK, Campos LT, Costa PR. Assessment of organ absorbed doses in patients undergoing chest X-ray examinations by Monte Carlo based softwares and phantom dosimetry. Radiat Meas. 2011; 46(12): 1981–4. https://doi.org/10.1016/j.radmeas.2011.07.017

[15] Yamashita K, Higashino K, Hayashi H, Takegami K, Hayashi F, Tsuruo Y, et al. Direct measurement of radiation exposure dose to individual organs during diagnostic computed tomography examination. Sci Rep. 2021; 11: 5435. https://doi.org/10.1038/s41598-021-85060-5

[16] Akyea-Larbi KO, Hasford F, Inkoom S, Tetteh MA, Gyekye PK. Evaluation of organ and effective doses using anthropomorphic phantom: a comparison between experimental measurement and a commercial dose calculator. Radiography. 2024; 30(1): 1–5. https://doi.org/10.1016/j.radi.2023.10.003

[17] Sina S, Mirzaiee F, Padargani T, Zehtabian M, Ahrari S. Radiation dose assessment in diagnostic imaging using thermoluminescent dosimeter-100H dosimeters and a RANDO phantom: insights from chest, pelvic, and skull examinations. J Med Phys. 2025; 50(2): 385–90. https://doi.org/10.4103/jmp.jmp_39_25

[18] Elamri N, Mkimel M, et al. Dose assessment in diagnostic radiography and risk probability for four procedures using digital radiography in a Moroccan hospital. Radiat Phys Chem. 2025; 235: 112892.

[19] Layal J, Mohammed A, Mohammed A, Abdelmoneim S. Patients' radiation dose evaluation during contrast enhanced computed tomography urography procedure. Radiat Phys Chem. 2024; 216: 111348. https://doi.org/10.1016/j.radphyschem.2023.111348

[20] Zira JD. Establishment of diagnostic reference levels for radiological procedures in selected teaching hospitals in north eastern Nigeria. J Radiogr Radiol Sci. 2018; 2: 49.

[21] Bullus S, Bajoga AD, Seydou H, Ijudigal J. Evaluation of radiation doses due to patients undergoing radiographic examinations at two public hospitals in Damaturu, Yobe State, Northeast Nigeria. 2022.

[22] Odunayo KO. Estimation of patient radiation doses for selected X-ray examinations and centres in north-central Nigeria [MTech thesis]. Minna: Federal University of Technology; 2021.

[23] Suliman II, Halato MA, Badawi AA, Sulieman AA, Gassom GA, Barsham MA, et al. Radiation doses in intravenous urography and potentials for optimization. In: Proceedings of the Tenth Radiation Physics and Protection Conference; 2010; Cairo, Egypt.

[24] Tukur YM, Salisu AM, Joseph IA, Jamilu AY. Assessment of entrance surface dose and effective dose in intravenous urography (IVU) procedure in selected hospitals in Yobe State, Nigeria. Commun Phys Sci. 2026; 13(1): 115–23. https://doi.org/10.4314/cps.v13i1.9

[25] International Atomic Energy Agency. Dosimetry in diagnostic radiology: an international code of practice. Technical Reports Series No. 457. Vienna: IAEA; 2007.

[26] International Commission on Radiological Protection. The 2007 recommendations of the International Commission on Radiological Protection. ICRP Publication 103. Ann ICRP. 2007; 37(2–4).

[27] International Commission on Radiological Protection. Radiation detriment calculation methodology. ICRP Publication 152. Ann ICRP. 2022; 51(3).

[28] Ban N, Cléro E, Vaillant L, Zhang W, Hamada N, Preston D, et al. Radiation detriment calculation methodology: summary of ICRP Publication 152. J Radiol Prot. 2022; 42(2): 023001.

[29] Cléro E, Vaillant L, Hamada N, Zhang W, Preston D, Laurier D, et al. History of radiation detriment and its calculation methodology used in ICRP Publication 103. J Radiol Prot. 2019; 39(3): R19–R35.

[30] United States Environmental Protection Agency. Guidelines for carcinogen risk assessment. EPA/630/P-03/001F. Washington (DC): Office of Research and Development; 2005.

[31] Joint Committee for Guides in Metrology. Evaluation of measurement data — guide to the expression of uncertainty in measurement. JCGM 100:2008. Sèvres: BIPM; 2008.

[32] International Commission on Radiological Protection. Diagnostic reference levels in medical imaging. ICRP Publication 135. Ann ICRP. 2017; 46(1).